

Numerical Simulation of a Planar Model of a Ball Absorber in a Spherical Dish

Marek Kawulok^{1,2*}, Stanislav Pospisil^{1,2}, Nela Freiherrova¹, David Juracka¹

¹ Department of Structural Mechanics, Faculty of Civil Engineering, VSB-Technical University of Ostrava, Ludvika Podeste 1875/17, 708 00 Ostrava-Poruba, Czech Republic

² Institute of Theoretical and Applied Mechanics, Czech Academy of Sciences, Prosecka 809/76, 190 00 Prague 9, Czech Republic

* Corresponding author, e-mail: marek.kawulok@vsb.cz

Received: 20 December 2022, Accepted: 20 April 2023, Published online: 08 May 2023

Abstract

This paper aims to investigate the behavior of a spherical absorber composed of two parts, an inner sphere and a supporting convex spherical dish in which the ball is placed. Considering only the planar behavior of the system, a set of governing nonlinear differential equations was derived and solved numerically. Firstly, the system is exposed to the harmonic excitation of the supporting bowl and its time response is analyzed for all time dependent variables. By gradually changing the angular frequency of the excitation, a resonance curve is obtained, which is examined in detail with respect to the changing amplitudes of the excitation force and the nonlinear behavior. The effect of internal damping and different settings of the absorber characteristics are also investigated. The effect of initial conditions without the presence of an external excitation force is also numerically analyzed by means of phase portraits for selected pairs of initial conditions.

Keywords

ball absorber, numerical analysis, time response analysis, resonance curve, phase portraits

1 Introduction

Structures are typically subjected to mechanical vibrations, classified according to their origin, as technologically, traffic or naturally induced, e.g., due to the influence of seismicity and wind. A structural engineer should try to minimize the effects of vibrations, to limit the damage to the structure, and to ensure the safe and comfortable use of the building by the occupants. For this purpose, damping devices are often integrated into load bearing systems to prevent excessive vibrations. The most widely used type is the passive absorber, by far. This is a mechanical device that dissipates energy from external sources and reduces the response of the structure [1].

An example of a passive damping device is the so-called spherical vibration absorber. An absorber of this type consists of an assembly of a supporting convex spherical canopy (dish) and a sphere rolling on this surface. The advantage of this type of absorber is the wide range of frequencies to which the absorber can be tuned by adjusting the radius of curvature of the surface, the diameter of the sphere, and the mass of the sphere. The absorber requires no daily maintenance to operate and, due to its size, nor

the large construction space. It finds applications in the field of structural dynamics, for example in the design of linear structures with large spans (bridges, footbridges) and tall slender buildings and structures (towers). Among all possible applications, absorbers can be used, for example, in towers [2] or wind turbines [3].

However, despite all these advantages, there are difficulties in the analytical and numerical analysis of the system. Although the system may appear to be similar to a pendulum whose boundary conditions are only holonomic, in the case of a spherical absorber, the boundary conditions are also functions of the derivatives of the position (velocity). A system with these boundary conditions is called non-holonomic. Publications dealing with the analysis of the spherical absorber have appeared only in recent decades. Pirner, Naprstek, and Fischer are the pioneers. In their publications, they point out motion instabilities, bifurcations, and difficulties associated with auto-parametric oscillations [4]. They also state that increased absorber efficiency due to higher energy losses can lead to the formation of chaotic zones in certain frequency bands [5].

These zones are induced by the nonlinear nature of the system with ambiguously defined regions. The effect of increasing radially rolling friction on the model behavior is studied in [6].

This work is focused on numerical simulations of the behavior of such a spherical absorber. The motion equations are derived by the methods of analytical mechanics. The Lagrange's equations are converted into a state-space formulation for implementation in mathematical software. The fields of interest include the time response of the structure to harmonic excitation. The object of the analysis is to calculate the resonance curves for different amplitudes of the excitation force and other parameters in order to monitor changes in these curves. Another objective is to analyze the effect of initial conditions on the behavior of a dynamic system without the influence of an external excitation force. For these purposes, phase portraits are created, see for instance [7]. Another key part of the analysis is to identify the location and nature of the fixed points in the phase space.

2 Derivation of the system of governing equations

In this section, a system of governing differential equations is derived based on the work of Náprstek et al. [5] and the same Lagrangian approach is used. The analyzed absorber consists of two components. A spherical bowl and a sphere, which is placed on it. In the case where the motion is restricted to a planar problem, the behavior of the dynamic system in time can be expressed in terms of the displacement of the support structure $u(t)$ and the angle $\varphi(t)$ indicating the position of the sphere. The zero value of the angle corresponds to the center of the bowl. As the description implies, this is a two-degrees-of-freedom problem, which is additionally excited by the force $F(t)$ to analyze the time response and to generate the resonance curves. This time-varying force is applied to the support structure, as can be seen in the schematic representation in Fig. 1.

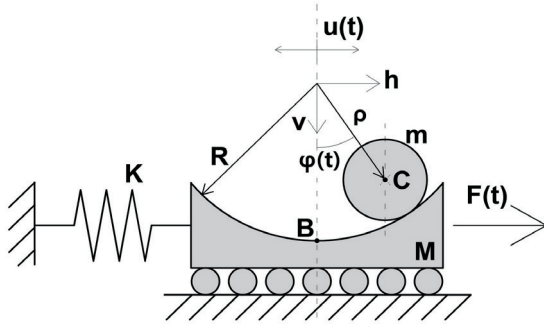


Fig. 1 Schematic planar representation of the analyzed spherical absorber system

The behavior of the system is determined by parameters including the mass of the support structure M , the mass of the sphere m , the spring stiffness K and ρ , indicating the distance between the centre of curvature of the bowl and the centre of the sphere. The calculation of ρ is therefore given by:

$$\rho = R - r, \tag{1}$$

where R is the radius of curvature of the support bowl and r is the radius of the sphere. Points C and B marks the center of the sphere and the bottom of the dish, respectively. A more detailed schematic representation of the inner sphere is shown in Fig. 2. In addition to the characteristics mentioned above, the diagram also shows the point P indicating the point of contact between the sphere and the bowl, the point Q lying on the surface of the sphere and the angle ψ . Value of the ψ represents the angle that point Q has travelled from the start of the rolling motion from point B . The value of this angle is measured from the vertical line passing through the center of the ball. The zero value of ψ is reached if $Q = P = B$. The angle ψ can be expressed from geometric relations as:

$$R\varphi = r\psi + r\varphi \rightarrow r\psi = \rho\varphi. \tag{2}$$

Before starting to derive the system of governing equations, the constraints must be introduced. For the absorber, the following derivation is based on two constraints. The first constraint states that the ball cannot disconnect itself from the bowl. This condition is represented by Eq. (1). The second constraint assumes sufficient friction between the sphere and the bowl. According to this condition, the ball still performs a rolling motion and cannot slip. The second condition is given by Eq. (2). If either condition is violated, the governing equations derived in this section would change.

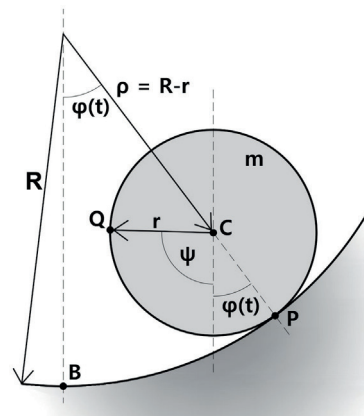


Fig. 2 Schematic illustration of the moving ball

In the following derivation, the time dependence labels will be dropped, that means $u(t) = u$, $\varphi(t) = \varphi$ and $F(t) = F$. Taking into account the notation of Fig. 1 and Fig. 2, the displacement of the center of the sphere can be expressed using the following equations:

Horizontal h direction:

$$h = \sin(\varphi)\rho + u. \quad (3)$$

Vertical v direction:

$$v = \cos(\varphi)\rho. \quad (4)$$

The derivation of these equations by time gives the velocity components in:

Horizontal h direction:

$$\dot{h} = \rho \cos(\varphi)\dot{\varphi} + \dot{u}. \quad (5)$$

Vertical v direction:

$$\dot{v} = -\rho \sin(\varphi)\dot{\varphi}. \quad (6)$$

With Eqs. (5) and (6), it is possible to derive the kinetic energy E . This consists of the kinetic energy of motion of the centre of the sphere and the supporting bowl. The rolling motion of the ball must also be included in the kinetic energy. This results in the following expression:

$$E = \frac{1}{2}m\left(\left(\rho \cos(\varphi)\dot{\varphi} + \dot{u}\right)^2 + \left(-\rho \sin(\varphi)\dot{\varphi}\right)^2\right) + \frac{1}{2}J\dot{\psi}^2 + \frac{1}{2}M\dot{u}^2, \quad (7)$$

$$J = \frac{2}{5}mr^2, \quad (8)$$

in which J is the moment of inertia, which is given for a sphere by Eq. (8). Combining Eqs. (7), (8), and (2) the kinetic energy can be determined:

$$E = \frac{7}{10}m\rho^2\dot{\varphi}^2 + \frac{1}{2}M\dot{u}^2 + m\rho \cos(\varphi)\dot{\varphi}\dot{u} + \frac{1}{2}m\dot{u}^2. \quad (9)$$

The potential energy of the system is the sum of gravitational potential energy and the elastic potential energy. Therefore, it can be written as follows:

$$V = mg\rho(1 - \cos(\varphi)) + \frac{1}{2}Ku^2. \quad (10)$$

To derive a system of governing equations, the effect of damping C should be included. In this case, the Rayleigh function in which c_φ and c_u are the coefficients will be considered. The same damping was used by the authors of the publication [5].

$$C = \frac{1}{2}m\rho^2c_\varphi\dot{\varphi}^2 + \frac{1}{2}Mc_u\dot{u}^2, \quad (11)$$

The principles of Lagrangian mechanics and Lagrange's equations of the second kind are used to derive the system of governing equations. The D'Alembert principle allows to write the equations of motion for the holonomic system in the form:

$$\frac{d}{dt}\left(\frac{\partial L}{\partial \dot{q}_i}\right) - \frac{\partial L}{\partial q_i} = Q_i, \quad (12)$$

in which q_i , \dot{q}_i and Q_i are generalized coordinates, generalized velocities and generalized forces, respectively. The Lagrange function appearing in Eq. (12) is defined as:

$$L = E - V. \quad (13)$$

In the case of the analyzed problem, we consider the system as non-conservative because there is a Rayleigh dissipation function and an external force excitation. Both of these components belong to generalized forces. The right-hand side of Eq. (12) is therefore in the following form:

$$Q_i = -\frac{\partial C}{\partial \dot{q}_i} + Q_i^{(F)}, \quad (14)$$

where $Q_i^{(F)}$ is the generalized force representing the external excitation. By making a few mathematical manipulations and combining Eqs. (12) and (14), we obtain the resulting Eq. (15), which will be used for further derivations.

$$\frac{d}{dt}\left(\frac{\partial L}{\partial \dot{q}_i}\right) - \frac{\partial L}{\partial q_i} + \frac{\partial C}{\partial \dot{q}_i} = Q_i^{(F)}. \quad (15)$$

For analyzed problem, $q_1 = \varphi$ and $q_2 = u$ are chosen. Hence, on the right-hand side of the equation $Q_1^{(F)} = 0$ and $Q_2^{(F)} = F$. By substituting the kinetic energy Eq. (9), potential energy Eq. (10) and Rayleigh damping Eq. (11) in Eq. (15), a system of two differential equations is derived in the form:

$$\left(\frac{7}{5}\rho\ddot{\varphi} + \rho c_\varphi\dot{\varphi} + g \sin(\varphi) + \cos(\varphi)\ddot{u}\right)m\rho = 0, \quad (16)$$

$$m\rho \cos(\varphi)\ddot{\varphi} - m\rho \sin(\varphi)\dot{\varphi}^2 + M\ddot{u} + m\ddot{u} + Mc_u\dot{u} + Ku = F \quad (17)$$

Eqs. (16) and (17) can be modified further. After some mathematical operations and simplification by introducing new constants defined as in Eqs. (20), (21), and (22), the equations can be written in the following forms:

$$\frac{7}{5}\ddot{\varphi} + c_\varphi\dot{\varphi} + \omega_m^2 \sin(\varphi) + \frac{1}{A}\cos(\varphi)\ddot{u} = 0, \quad (18)$$

$$\eta\rho\cos(\varphi)\ddot{\varphi} - \eta\rho\sin(\varphi)\dot{\varphi}^2 + (1+\eta)\ddot{u} + c_u\dot{u} + \omega_M^2 u = \frac{F}{M}, \quad (19)$$

$$\omega_m^2 = \frac{g}{\rho}, \quad (20)$$

$$\omega_M^2 = \frac{K}{M}, \quad (21)$$

$$\eta = \frac{m}{M}. \quad (22)$$

The system of nonhomogeneous nonlinear coupled differential equations of the second order Eqs. (18) and (19) represent the governing equations that describe the motion of an excited spherical absorber placed in a spherical bowl.

3 Numerical simulations

In this section, the derived system of governing differential Eqs. (15) and (16) is subjected to numerical solution. MATLAB software was used to perform the numerical simulations. It features tools for solving differential equations of ODEs. Stiff solvers ODE15s, ODE23s, ODE23t, ODE23tb, and non-stiff solvers ODE23, ODE113, ODE78, ODE89, and ODE45 are available in the software [8]. A comparison of some of the mentioned solvers for dynamic systems with impact can be found in [9] and a comparison of software that allows numerical solution of differential equations can be found in [10].

For the analyzed system of differential equations, the ODE45 solver was chosen. It is a non-stiff solver with good accuracy and is recommended as a first solver in the calculation of the equations. ODE45 is based on the Dormand-Prince pair, which belongs to the explicit methods and to the Runge-Kutta solvers. It is obtained by simultaneous implementation of fourth and fifth order Runge-Kutta formula [11]. To compute the search value using this approach, knowledge of the initial functional value is required. In the first step, these are the initial conditions. This is a one-step solver.

To solve, the system of two second-order differential equations must be converted to a system of four first-order differential equations. Displacement components and their time derivatives are converted into a vector and denoted by the unknown x_1 to x_4 .

$$\begin{pmatrix} x_1 \\ x_2 \\ x_3 \\ x_4 \end{pmatrix} = \begin{pmatrix} \varphi \\ \dot{\varphi} \\ u \\ \dot{u} \end{pmatrix}. \quad (23)$$

By deriving Eq. (23) with respect to time, we get the vector:

$$\begin{pmatrix} \dot{x}_1 \\ \dot{x}_2 \\ \dot{x}_3 \\ \dot{x}_4 \end{pmatrix} = \begin{pmatrix} \dot{\varphi} = x_2 \\ \ddot{\varphi} \\ \dot{u} = x_4 \\ \ddot{u} \end{pmatrix}. \quad (24)$$

The velocities $\dot{\varphi}$ and \dot{u} appear in Eq. (24). However, these can be written according to Eq. (23) as $\dot{\varphi} = x_2$ and $\dot{u} = x_4$. The acceleration components and have to be expressed from Eqs. (18) and (19). Using the notation according to Eq. (23), the following expressions are obtained:

$$\ddot{\varphi} = \frac{+ (5\eta M \rho \sin(x_1) x_2^2 - (5c_u x_4 + 5\omega_M^2 x_3) M + 5F) \cos(x_1) - 5M\rho(\eta-1)(\omega_m^2 \sin(x_1) + c_\varphi x_2)}{\rho M (5\eta \cos^2(x_1) + 7\eta - 7)}, \quad (25)$$

$$\ddot{u} = \frac{-7\eta\rho M \sin(x_1) x_2^2 + (7c_u x_4 + 7\omega_M^2 x_3) M - 7F - 5\rho M \eta (\omega_m^2 \sin(x_1) + c_\varphi x_2) \cos(x_1) - M (5\eta \cos^2(x_1) + 7\eta - 7)}{M (5\eta \cos^2(x_1) + 7\eta - 7)}. \quad (26)$$

The resulting relations from Eq. (24) with the addition of Eqs. (25) and (26) give a state-space formulation that can be solved using the ODE45 solver in MATLAB software.

Simulations are performed for a system of a supporting spherical canopy and a ball defined by $m = 1$ kg, $M = 7$ kg, $\rho = 0.7$ m, $K = 145$ N/m. The damping coefficients are chosen as $c_\varphi = 0.15$ and $c_u = 0.25$. In the case of the analysis of the response of the damper in time and for the generation of resonance curves, a periodic excitation is applied to the support bowl:

$$F = F_0 \sin(\omega t), \quad (27)$$

where F_0 is the amplitude of the excitation force and ω is the excitation angular frequency.

3.1 Time response to excitation force

With the completed state space formulation, it is possible to proceed to the numerical calculation. The subject of the first analysis is the time response of the unknown components to a periodic excitation described by Eq. (27) with force amplitude $F_0 = 5$ N and excitation angular frequency $\omega = 2.9$ rad/s, i.e., with the period $T = 2.17$ s. The initial conditions are assumed to be zero for these calculations and only the excitation force is considered. The oscillatory response of the absorber is simulated for the time duration of 120 s. The length of the time interval was chosen

so that both transient and steady state response could be observed. The resulting values are presented graphically for angle φ (Fig. 3) and displacement u (Fig. 4). For the velocity components ($\dot{\varphi}$ and \dot{u}), the same behavior can be observed at a given scale; their graphical representation has been omitted in this case.

It can be seen from the graphs, that while the support structure oscillates with large displacement amplitudes at the beginning of the transient response, the inner ball begins to increase its displacement (time approximately 0–30 s). As the amplitudes of the ball response increase, the response of the support structure begins to decrease (time approximately 30–60 s). This increasing trend is reversed towards the end of the transient response (time approximately 60–90 s) and the response components stabilize (time from 90 s). In Fig. 5 and Fig. 6, it is possible

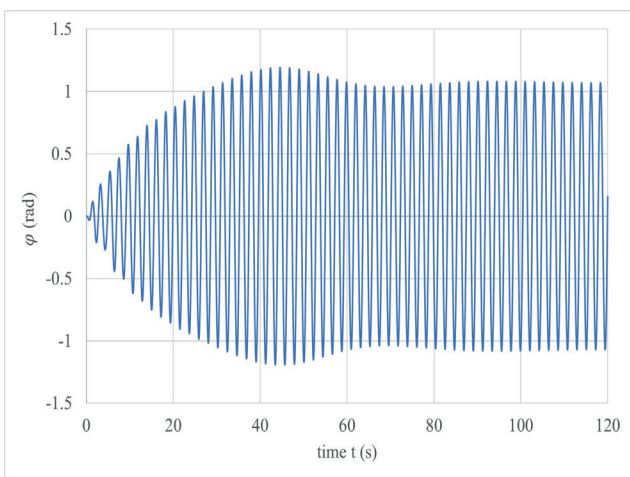


Fig. 3 Time response of angle φ to harmonic excitation with force amplitude $F_0 = 5$ N and angular frequency 2.9 rad/s

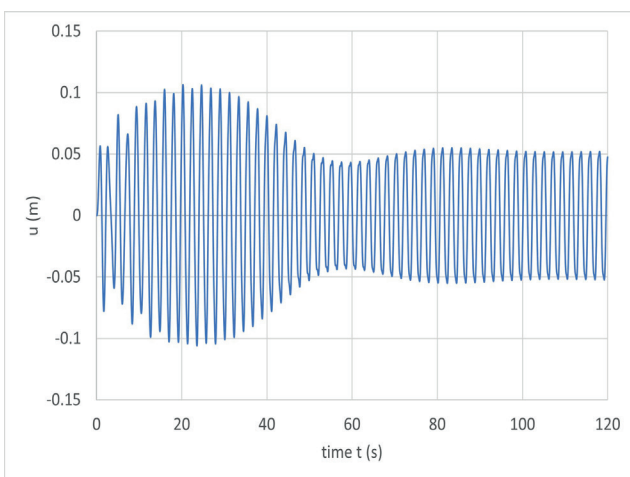


Fig. 4 Time response of displacement u to harmonic excitation with force amplitude $F_0 = 5$ N and angular frequency 2.9 rad/s

to observe the changes in displacement and velocity of the support structure in the time window from 30 to 70 s.

If we increase the excitation angular frequency to $\omega = 4.5$ rad/s, we can observe in Figs. 7–8 that resonance has occurred in both components of the absorber. In the next part of the analysis, the focus is on the generation of resonance curves.

3.2 Resonance curves

The resonance curves for the angle φ and the displacement of the support structure u represent the relation between the absolute value of the response amplitude for a given force and an excitation angular frequency. Their derivatives are considered to follow the same trend, as the following equations hold:

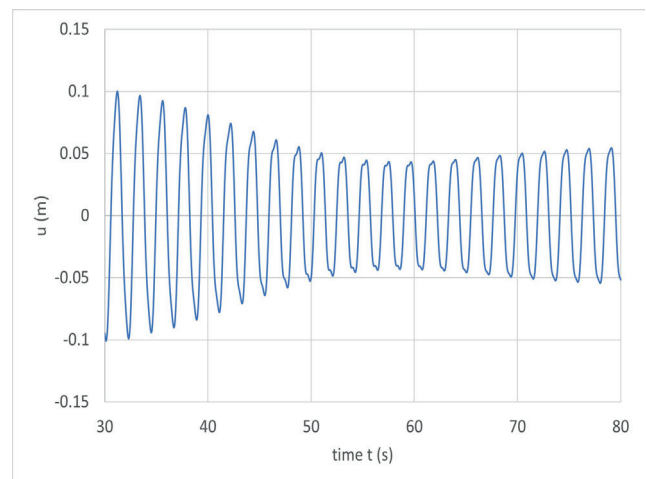


Fig. 5 Detail of time response of displacement u to harmonic excitation with force amplitude $F_0 = 5$ N and angular frequency 2.9 rad/s in the time window from 30 s to 70 s

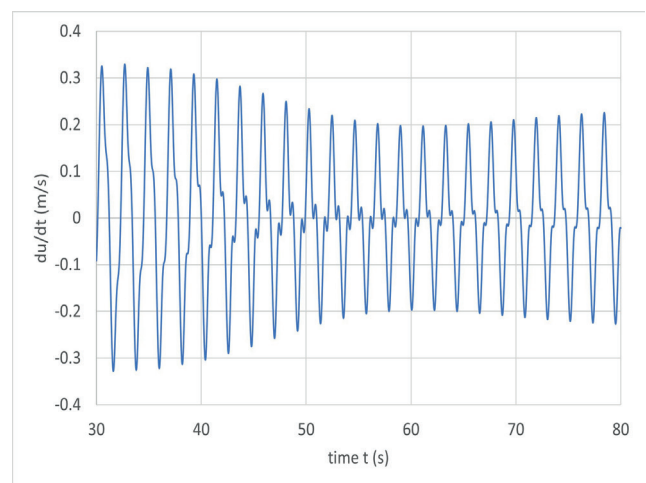


Fig. 6 Detail of time response of velocity \dot{u} to harmonic excitation with force amplitude $F_0 = 5$ N and angular frequency 2.9 rad/s in the time window from 30 s to 70 s

$$\frac{\varphi_{j,max}}{\dot{\varphi}_{j,max}} \omega_j = constant, \tag{28}$$

$$\frac{u_{j,max}}{\dot{u}_{j,max}} \omega_j = constant. \tag{29}$$

In Eqs. (28) and (29), ω is the excitation angular frequency to obtain the j -th time response. By analyzing the time response for a given value of ω_j , the maximum values of response $\omega_{j,max}$ and angular velocity $\dot{\omega}_{j,max}$ are obtained. The ratio of $\omega_{j,max}$ and $\dot{\omega}_{j,max}$ multiplied by ω_j is equal to a constant. This constant should be the same for all j . The same is true for the maximum response $u_{j,max}$ and the velocity $\dot{u}_{j,max}$. Their ratio multiplied by the corresponding angular frequency is equal to a constant that is the same for all j . To construct the resonance curve, the excitation angular frequency is stepwise varied by a step size of 0.001 rad/s over a range of 2 to 6 rad/s. Thus, a total of

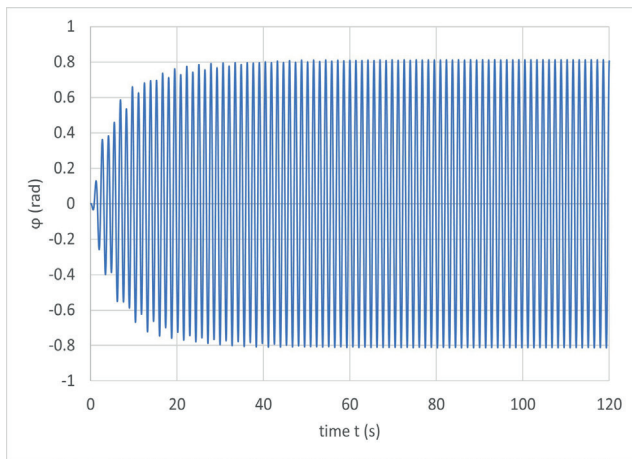


Fig. 7 Time response of angle φ to harmonic excitation with force amplitude $F_0 = 5$ N and angular frequency 4.5 rad/s

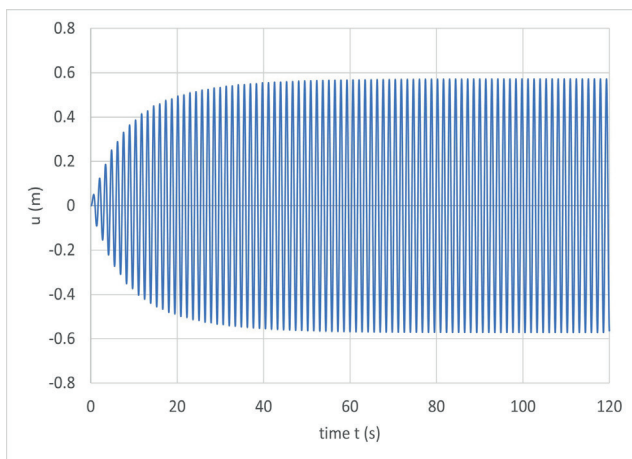


Fig. 8 Time response of displacement u to harmonic excitation with force amplitude $F_0 = 5$ N and angular frequency 4.5 rad/s

4001 simulations have been performed. Considering the number of parameters entering the simulation, a study of their influence on the shape of the resonance curve is carried out in the following text.

Firstly, the effect of the excitation force amplitude described by Eq. (27) is analyzed. Calculations are carried out for a total of five different amplitudes $F_0 = 1, 2, 3, 4$ and 5 N. The remaining parameters are constants ($m = 1$ kg, $M = 7$ kg, $\rho = 0.7$ m, $K = 145$ N/m, $c_\varphi = 0.15$ and $c_u = 0.25$). The results of the calculations performed for the dependence between the excitation angular frequency and the displacement u or angle φ are plotted in Figs. 9 and 10, respectively. The colors and line types in these figures correspond to different amplitudes of the excitation force. In these simulations, two local maxima can be seen around 3 rad/s and 4.55 rad/s. When these peaks, it can be noticed

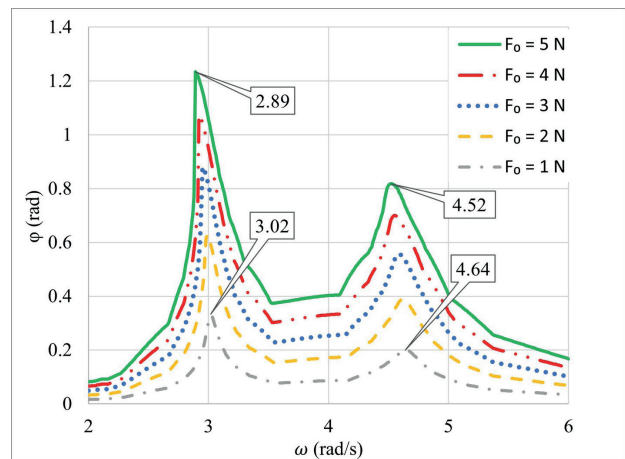


Fig. 9 Resonance curve for angle φ with different excitation amplitudes $F_0 = 1, 2, 3, 4$ and 5 N. The box indicates the omega value at which the maximum response was determined

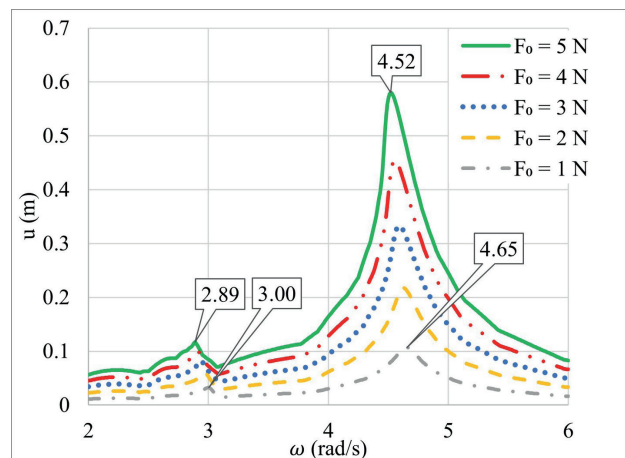


Fig. 10 Resonance curve for displacement u with different excitation amplitudes $F_0 = 1, 2, 3, 4$ and 5 N. The box indicates the omega value at which the maximum response was determined

that as the excitation amplitude increases, the excitation angular frequency at which this value is reached changes. For example, for an excitation force of $F_0 = 1$ N, the first peak value of the response is reached for angle φ with an excitation $\omega_1 = 3.02$ rad/s and the second peak value with $\omega_2 = 4.64$ rad/s. These angular frequencies are different compared to $\omega_1 = 2.89$ rad/s and $\omega_2 = 4.52$ rad/s for excitation force $F_0 = 5$ N. As the excitation force increases, there is a softening behaviour of the resonance curve [12]. In the previous section focusing on the time response, the excitation force with amplitude $F_0 = 5$ N and excitation angular frequency ω were selected with purpose to observe the absorber behaviour in these regions of maximum response.

Damping is an important factor in the simulation. The internal damping in the case of the analyzed dynamic is modelled using the Rayleigh dissipation function described by Eq. (11). The coefficients c_φ and c_u are present in this equation. In this section, their influence on the shape of the resonance curves will be analyzed. The remaining input parameters are $m = 1$ kg, $M = 7$ kg, $\rho = 0.7$ m, $K = 145$ N/m and $F_0 = 3$ N. In Figs. 11 and 12, the shapes of the curves can be seen for varying the value of $c_\varphi = 0.1, 0.2, 0.3, 0.4$ and 0.5 while the value of $c_u = 0.25$ remains constant. From the graph in Fig. 11 (response φ), it can be observed that there are significant changes in the maximum value of the amplitude reached around the excitation angular frequency of $\omega_1 = 3$ rad/s. Only small changes are observed around the second maximum at $\omega_2 = 4.55$ rad/s. For the resonance curve for the u component, there is a decrease in response around both resonances. A different behavior can be observed when the coefficient c_u is changed. Here, in Fig. 13 and Fig. 14, significant changes can be observed

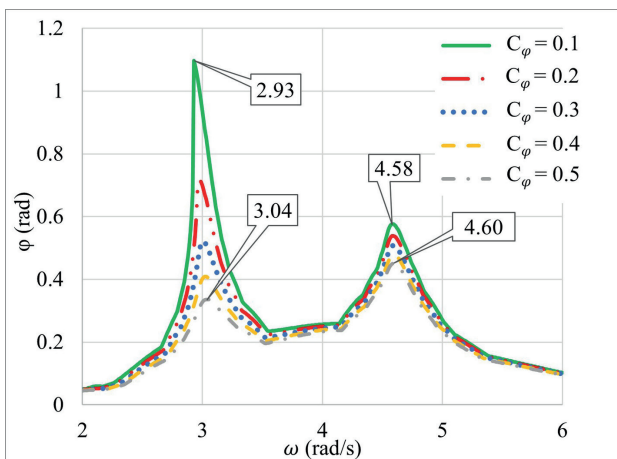


Fig. 11 Resonance curve for angle φ with different coefficients $c_\varphi = 0.1, 0.2, 0.3, 0.4$ and 0.5 . The box indicates the omega value at which the maximum response was determined

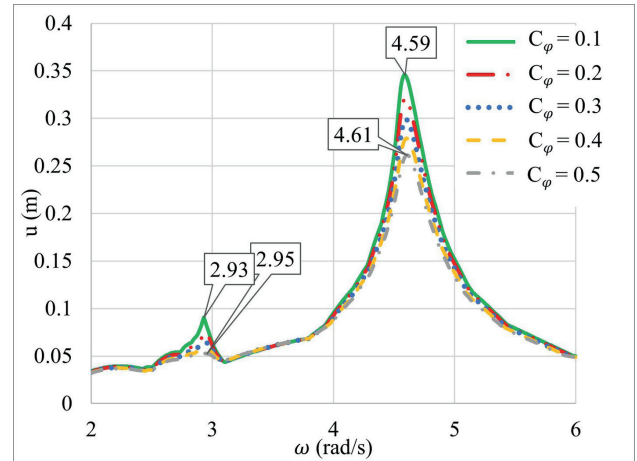


Fig. 12 Resonance curve for displacement u with different coefficients $c_\varphi = 0.1, 0.2, 0.3, 0.4$ and 0.5 . The box indicates the omega value at which the maximum response was determined

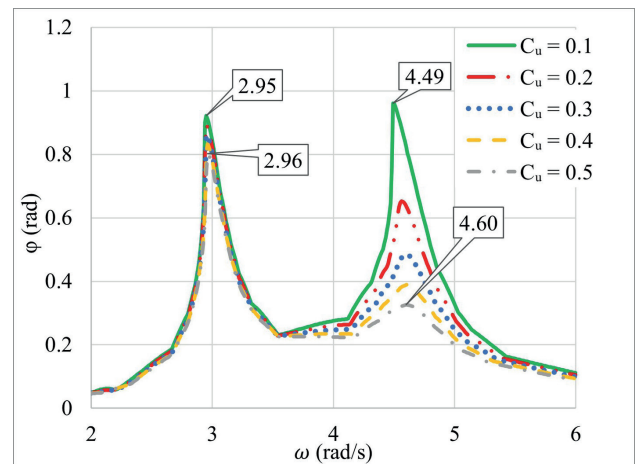


Fig. 13 Resonance curve for angle φ with different coefficients $c_u = 0.1, 0.2, 0.3, 0.4$ and 0.5 . The box indicates the omega value at which the maximum response was determined

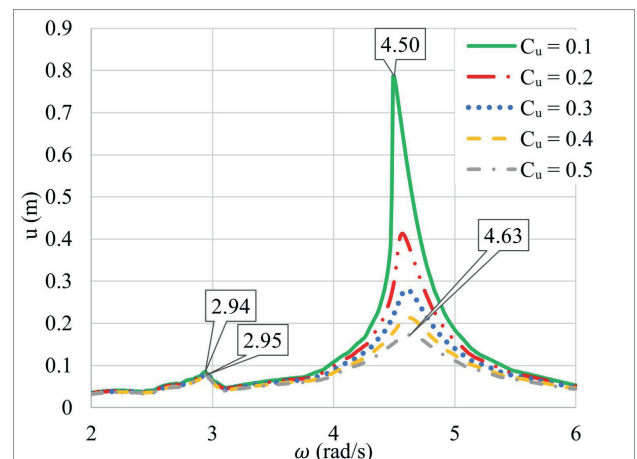


Fig. 14 Resonance curve for displacement u with different coefficients $c_u = 0.1, 0.2, 0.3, 0.4$ and 0.5 . The box indicates the omega value at which the maximum response was determined

around the excitation angular frequency of 4.55 rad/s and almost none at $\omega_1 = 3$ rad/s. These graphs show the resonance curves for $c_u = 0.1, 0.2, 0.3, 0.4$ and 0.5 , while $c_\varphi = 0.15$. In both cases, softening of the resonance curves can be observed.

Another parameter whose influence is analyzed is the mass of the support structure M . The masses $M = 6, 7, 8, 9$ and 10 kg were selected for analysis. Other parameters remain unchanged. The resonance curves for the angle φ are plotted in Fig. 15. It can be seen from the plot that with increasing mass, there is an increase in the response in the region of the first maximum and a slight shift in the excitation angular frequency at which this maximum is reached. From $\omega_1 = 2.97$ rad/s ($M = 6$ kg) to $\omega_1 = 2.9$ rad/s ($M = 10$ kg). A similar behavior is observed for the second maximum value. Here, the amplitude of the response also increases. However, there is a larger shift in the angular excitation frequency at which the maximum response is reached. From a value of $\omega_2 = 4.92$ rad/s ($M = 6$ kg) to $\omega_2 = 3.91$ rad/s ($M = 10$ kg). An increase in the values of the amplitudes is also observed between these local maxima. The resonance curves for the displacement of the support structure u are plotted in Fig. 16. Even for the curves plotted on these graphs, there is a noticeable shift in the values of ω as the mass of the structure increases. In the case of the response u , a change in trend occurred at the second local maximum, where the maximum amplitude of the response decreases with increasing mass. In both response cases, it can be said that the values of the angular excitation frequencies ω_1 and ω_2 decrease with increasing mass of the support structure. Also, a trend of decreasing separation between these two angular frequencies with increasing mass M is observed.

The subject of the analysis is also the second mass, that is, the mass of the inner ball. This will be represented with the values $m = 1, 2, 3, 4$ and 5 kg. A graphical representation of the resonance curves for the response component φ is shown in Fig. 17. As can be seen in these plots, there is a reduction in response with increasing sphere mass. The changes also occur at the angular excitation frequency. For a sphere mass $m = 1$, kg, the values of $\omega_1 = 2.95$ rad/s and $\omega_2 = 4.59$ rad/s. As the mass of the sphere increases, these frequencies move away from each other, so for $m = 5$, kg, $\omega_1 = 2.67$ rad/s and $\omega_2 = 4.82$ rad/s. The separation of the angular frequencies is also visible in the resonance curves for the displacement component of the support structure u . These graphs are plotted in Fig. 18. The difference for this component can be seen

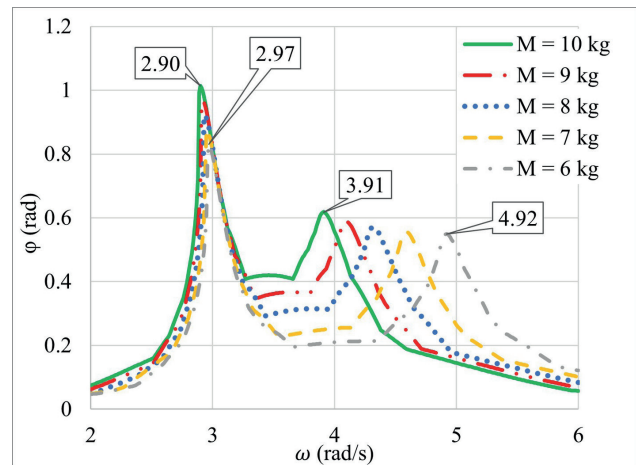


Fig. 15 Resonance curve for angle φ with different mass of the support structure $M = 6, 7, 8, 9$ and 10 kg. The box indicates the omega value at which the maximum response was determined

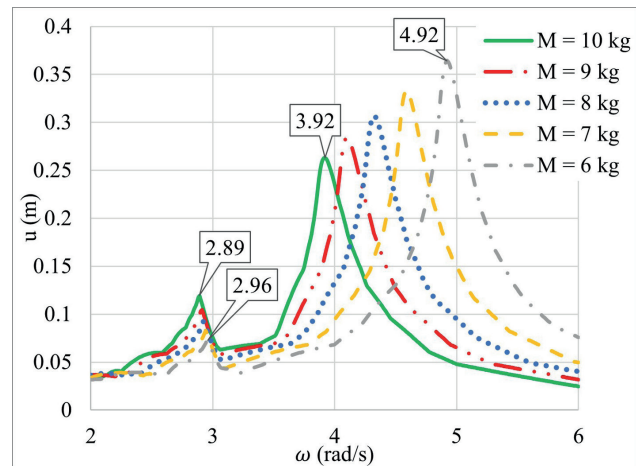


Fig. 16 Resonance curve for displacement u with different mass of the support structure $M = 6, 7, 8, 9$ and 10 kg. The box indicates the omega value at which the maximum response was determined

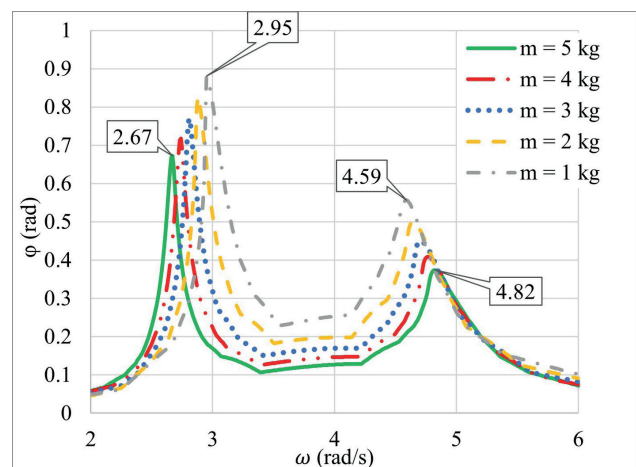


Fig. 17 Resonance curve for angle φ with different mass of the inner ball $m = 1, 2, 3, 4$ and 5 kg. The box indicates the omega value at which the maximum response was determined

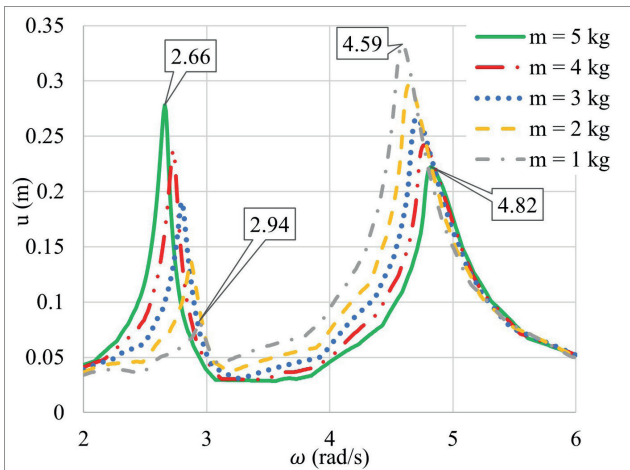


Fig. 18 Resonance curve for displacement u with different mass of the inner ball $m = 1, 2, 3, 4$ and 5 kg. The box indicates the omega value at which the maximum response was determined

in the region of the first local maximum. Here, there is an increase in the amplitude of the displacement response with increasing mass of the ball.

The last parameter analyzed is ρ . This parameter is described by Eq. (1). Numerical simulations were performed with values of $\rho = 0.6, 0.7, 0.8, 0.9$ and 1.0 m. The resulting resonance curves for φ can be found in the Fig. 19. It is worth to mention, that the response of the structure decreases with increasing value of ρ . The values of the excitation angular frequencies at which the maximum response was achieved also decrease with increasing ρ . In the case of the first maximum, there was a change from $\omega_1 = 3.13$ rad/s to $\omega_1 = 2.55$ rad/s. In the case of the second maximum, the change is not so significant, here the value dropped from $\omega_2 = 4.61$ rad/s to $\omega_2 = 4.55$ rad/s. For the response curves for u , shown in Fig. 20, a slight increase in response can be observed in the region of the second maximum. In contrast, when examining the first maximum, we can see that the response decreases with increasing ρ .

3.3 Local stability and phase portraits

This section deals with an examination of the system without the influence of external excitation. In the first part, fixed points will be searched, and then phase portraits will be constructed for selected pairs of initial conditions.

For a closer examination of the phase portraits, it is necessary to determine the fixed points of the dynamical system as first. The position of the fixed points is described as follows:

$$\frac{d}{dt} \mathbf{x} = \mathbf{f}(\mathbf{x}) = 0. \quad (30)$$

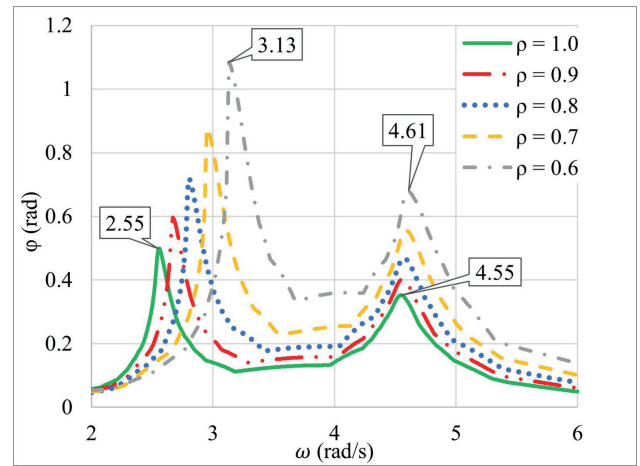


Fig. 19 Resonance curve for angle φ with parameter $\rho = 0.6, 0.7, 0.8, 0.9$ and 1.0 m. The box indicates the omega value at which the maximum response was determined

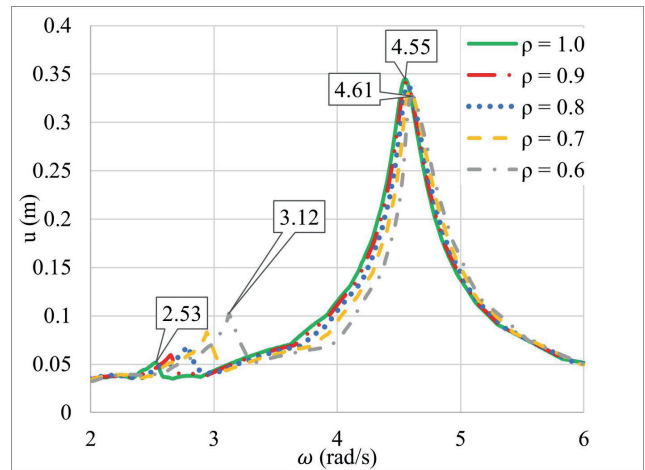


Fig. 20 Resonance curve for displacement u with parameter $\rho = 0.6, 0.7, 0.8, 0.9$ and 1.0 m. The box indicates the omega value at which the maximum response was determined

In the case of the analyzed absorber, Eq. (30) is written in the following form:

$$\frac{d}{dt} \begin{pmatrix} \varphi \\ \dot{\varphi} \\ u \\ \dot{u} \end{pmatrix} = \begin{pmatrix} 0 \\ 0 \\ 0 \\ 0 \end{pmatrix}. \quad (31)$$

If we modify the differential equations, Eqs. (18) and (19), with the omitted excitation term ($F = 0$ N), and substitute them into Eq. (31), we obtain the system of equations Eq. (31).

$$\dot{\varphi} = 0, \quad (32)$$

$$\ddot{\varphi} = \frac{+ (5\eta M \rho \sin(\varphi) \dot{\varphi}^2 - (5c_u \dot{u} + 5\omega_M^2 u) M) \cos(\varphi) - \rho M (5\eta \cos^2(\varphi) + 7\eta - 7)}{\rho M (5\eta \cos^2(\varphi) + 7\eta - 7)} \quad (33)$$

$$\frac{-5M\rho(\eta-1)(\omega_m^2 \sin(\varphi) + c_\varphi \dot{\varphi})}{\rho M (5\eta \cos^2(\varphi) + 7\eta - 7)} = 0, \quad (34)$$

$$\dot{u} = 0, \quad (34)$$

$$\ddot{u} = \frac{-7\eta\rho M \sin(\varphi) \dot{\varphi}^2 + (7c_u \dot{u} + 7\omega_M^2 u) M - M (5\eta \cos^2(\varphi) + 7\eta - 7)}{M (5\eta \cos^2(\varphi) + 7\eta - 7)} \quad (35)$$

$$\frac{-5\rho M \eta (\omega_m^2 \sin(\varphi) + c_\varphi \dot{\varphi}) \cos(\varphi)}{M (5\eta \cos^2(\varphi) + 7\eta - 7)} = 0.$$

By solving the system of equations defined by Eqs. (32), (33), (34) and (35) two fixed points were determined. Their location is described in Table 1, where k is an integer multiplier. For the absorber, only the nodes for $k = 0$ are relevant. Because the angle $\varphi = \pi$ for the sphere is physically impossible for this dish, no further analysis will be performed for this fixed point.

A closer study of fixed points will be based on the Hartman-Grobman theorem [13–14], which states that the behavior of a system in the neighborhood of hyperbolic fixed points is the same as the behavior of a linearized system near this point. To verify whether a nonlinear system can be linearized around a fixed point, it is necessary to verify that the fixed point is hyperbolic. The first step is to construct the Jacobian matrix of $f(\mathbf{x})$, where \mathbf{x} is the vector described by Eq. (23). The resulting matrix, named A , has the form:

$$A = \begin{bmatrix} \frac{\partial \dot{\varphi}}{\partial \varphi} & \frac{\partial \dot{\varphi}}{\partial \dot{\varphi}} & \frac{\partial \dot{\varphi}}{\partial u} & \frac{\partial \dot{\varphi}}{\partial \dot{u}} \\ \frac{\partial \ddot{\varphi}}{\partial \varphi} & \frac{\partial \ddot{\varphi}}{\partial \dot{\varphi}} & \frac{\partial \ddot{\varphi}}{\partial u} & \frac{\partial \ddot{\varphi}}{\partial \dot{u}} \\ \frac{\partial \dot{u}}{\partial \varphi} & \frac{\partial \dot{u}}{\partial \dot{\varphi}} & \frac{\partial \dot{u}}{\partial u} & \frac{\partial \dot{u}}{\partial \dot{u}} \\ \frac{\partial \ddot{u}}{\partial \varphi} & \frac{\partial \ddot{u}}{\partial \dot{\varphi}} & \frac{\partial \ddot{u}}{\partial u} & \frac{\partial \ddot{u}}{\partial \dot{u}} \end{bmatrix} = \begin{bmatrix} \frac{\partial \dot{x}_1}{\partial x_1} & \frac{\partial \dot{x}_1}{\partial x_2} & \frac{\partial \dot{x}_1}{\partial x_3} & \frac{\partial \dot{x}_1}{\partial x_4} \\ \frac{\partial \dot{x}_2}{\partial x_1} & \frac{\partial \dot{x}_2}{\partial x_2} & \frac{\partial \dot{x}_2}{\partial x_3} & \frac{\partial \dot{x}_2}{\partial x_4} \\ \frac{\partial \dot{x}_3}{\partial x_1} & \frac{\partial \dot{x}_3}{\partial x_2} & \frac{\partial \dot{x}_3}{\partial x_3} & \frac{\partial \dot{x}_3}{\partial x_4} \\ \frac{\partial \dot{x}_4}{\partial x_1} & \frac{\partial \dot{x}_4}{\partial x_2} & \frac{\partial \dot{x}_4}{\partial x_3} & \frac{\partial \dot{x}_4}{\partial x_4} \end{bmatrix}. \quad (36)$$

For a fixed point to be hyperbolic, all eigenvalues λ_i of the Jacobian matrix A must have a real part different from zero. Thus, we expect eigenvalues written in the following form:

$$\lambda_i = a \pm ib, \text{ where } a \neq 0. \quad (37)$$

The eigenvalues of matrix of the system, with the fixed point locations substituted, are:

From Table 2, it is clear that, in this case, it is a hyperbolic fixed point. Therefore, the nonlinear system of Eq. (30) can be linearized around this fixed point using the Jacobian matrix Eq. (36). The linearized system can be written as:

$$\frac{d}{dt} \mathbf{x} = A \mathbf{x}. \quad (38)$$

A closer analysis focuses on the initial conditions φ and $\dot{\varphi}$. The remaining initial conditions are zero. The neighborhood of the first fixed point is shown in Fig. 21. As can be seen from the graph or the eigenvalues, this is a stable fixed point, the so-called stable sink.

In the next section, the phase portraits for the taken pairs of initial conditions will be shown. For a given pair, the initial conditions will be taken randomly so that the behavior of the absorber and the supporting structure can be visualized. The first pair is the angle φ and the angular velocity $\dot{\varphi}$. Fig. 22 shows the phase portrait for initial conditions $\varphi = 1$ rad and $\dot{\varphi} = 1.5$ rad/s. This is followed by the phase portrait of the angle φ shift u . This is shown in

Table 1 Location of the fixed points

Fixed point	Location of fixed point			
	φ (rad)	$\dot{\varphi}$ (rad/s)	u (m)	\dot{u} (m/s)
1	$k 2\pi$	0	0	0
2	$k 2\pi + \pi$	0	0	0

Table 2 Eigenvalues of A determined on fixed points

Fixed point	Eigenvalues			
1	-0.05+3.03i	-0.05-3.03i	-0.13+4.66i	-0.13-4.66i

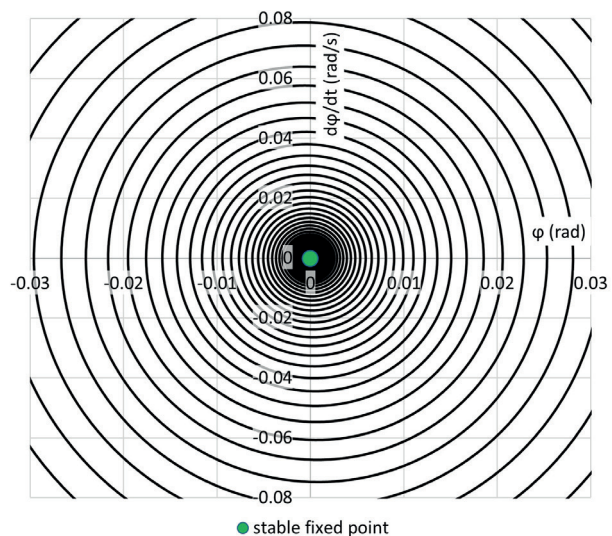


Fig. 21 The neighborhood of the stable fixed point with coordinates $\varphi = 0$ rad and $\dot{\varphi} = 0$ rad/s

Fig. 23 for $\varphi = 0$ rad and $u = 0.1$ m. The last phase portrait (Fig. 24) plots the relationship between φ and the velocity \dot{u} when $\varphi = 1$ rad and $\dot{u} = 0$ m/s.

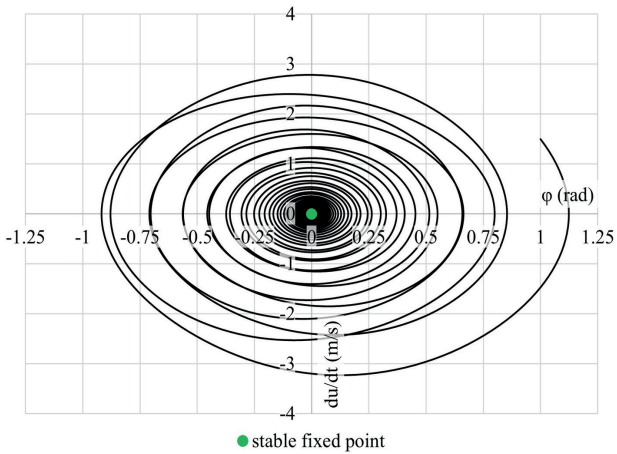


Fig. 22 Phase portrait with initial conditions $\varphi = 1$ rad and $\dot{\varphi} = 1.5$ rad/s

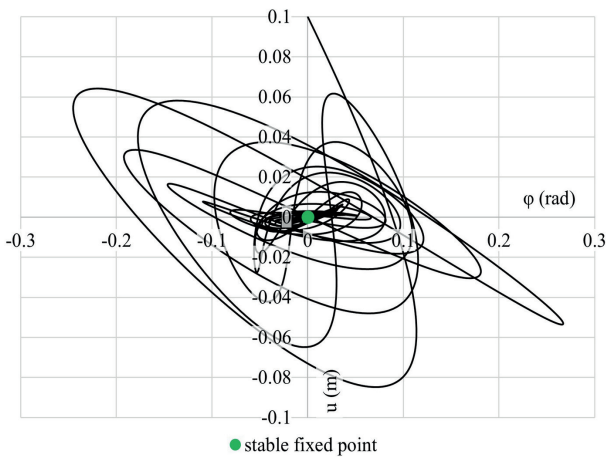


Fig. 23 Phase portrait with initial conditions $\varphi = 0$ rad and $u = 0.1$ m

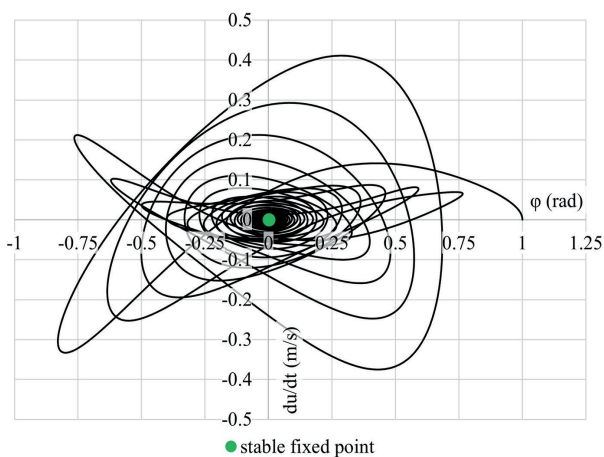


Fig. 24 Phase portrait with initial conditions $\varphi = 1$ rad and $\dot{u} = 0$ m/s

4 Conclusions

This paper is focused on the numerical simulations of the behavior of a spherical absorber placed in a supporting convex spherical dish. The derived system of two differential equations was converted to state space formulation and analyzed in MATLAB mathematical software. The first objective was to determine the time response of the system to harmonic excitation. The behavior for excitation with defined amplitude and two different excitation frequencies was described. In the first case, a transition between transient and steady-state responses was observed. However, in the second case, resonance occurred for both time-dependent variables.

Furthermore, the angular frequency of excitation was gradually increased for harmonic excitation, and resonance curves were generated for five different excitation amplitudes. Based on this analysis, a softening effect was observed for the resonance curves. Subsequent simulations focused on the effect of other parameters on the resonance curve. Among the analyzed factors were the damping function parameters, the mass of the support structure, the mass of the sphere, and the difference between the radius of curvature of the support bowl and the radius of the ball. Shifts in excitation angular frequency at which resonance occurred and changes in response amplitudes were observed in the resulting plots. The investigation of the effect of the initial conditions was carried out by creating phase portraits. This analysis also included the identification of fixed points. Recurrent fixed points with a period angle of π were revealed. However, only one point corresponding to the bottom of the bowl was chosen for further investigation, because the second point is not achievable for the case of a ball absorber. The stability determination was performed by linearization in the neighborhood of the detected fixed points. Phase portraits for a selected pair of initial conditions were also plotted to observe their interaction.

Future research by the author's team will focus on experimental verification of the mathematical models and the results obtained by numerical simulations.

Acknowledgement

The financial supports of the grant program financed by Ministry of Education, Youth and Sports of the Czech Republic through VSB–TUO SGS SP2022/43 and from the budget for conceptual development of science, research and innovations are highly acknowledged.

References

- [1] Elias, S., Matsagar, V. "Research developments in vibration control of structures using passive tuned mass dampers", *Annual Reviews in Control*, 44, pp. 129–156, 2017.
<https://doi.org/10.1016/j.arcontrol.2017.09.015>
- [2] Pirner, M. "Actual behaviour of a ball vibration absorber", *Journal of Wind Engineering and Industrial Aerodynamics*, 90(8), pp. 987–1005, 2002.
[https://doi.org/10.1016/S0167-6105\(02\)00215-5](https://doi.org/10.1016/S0167-6105(02)00215-5)
- [3] Chen, J., Georgakis, C. T. "Tuned rolling-ball dampers for vibration control in wind turbines", *Journal of Sound and Vibration*, 332(21), pp. 5271–5282, 2013.
<https://doi.org/10.1016/j.jsv.2013.05.019>
- [4] Náprstek, J., Fischer, C. "Stable and unstable solutions in auto-parametric resonance zone of a non-holonomic system", *Nonlinear Dynamics*, 99(1), pp. 299–312, 2020.
<https://doi.org/10.1007/s11071-019-04948-0>
- [5] Náprstek, J., Fischer, C., Pirner, M., Fischer, O. "Non-linear Model of a Ball Vibration Absorber", In: Papadrakakis, M., Fragiadakis, M., Plevris, V. (eds.) *Computational Methods in Earthquake Engineering*, Springer, 2013, pp. 381–396. ISBN: 978-94-007-6572-6
https://doi.org/10.1007/978-94-007-6573-3_18
- [6] Matta, E. "Ball vibration absorbers with radially-increasing rolling friction", *Mechanical Systems and Signal Processing*, 132, pp. 353–379, 2019.
<https://doi.org/10.1016/j.ymssp.2019.06.033>
- [7] Holmes, P., Rand, D. "Phase portraits and bifurcations of the non-linear oscillator: $\ddot{x} + (\alpha + \gamma x^2)\dot{x} + \beta x + \delta x^3 = 0$ ", *International Journal of Non-Linear Mechanics*, 15(6), pp. 449–458, 1980.
[https://doi.org/10.1016/0020-7462\(80\)90031-1](https://doi.org/10.1016/0020-7462(80)90031-1)
- [8] Omale, D., Ojih, P. B., Ogwo, M. O. "Mathematical Analysis of Stiff and Non-Stiff Initial Value Problems of Ordinary Differential Equation Using Matlab", *International Journal of Scientific & Engineering Research*, 5, pp. 49–59, 2014.
- [9] Dallas, S., Machairas, K., Papadopoulos, E. "A Comparison of Ordinary Differential Equation Solvers for Dynamical Systems With Impacts", *Journal of Computational and Nonlinear Dynamics*, 12(6), 061016, 2017.
<https://doi.org/10.1115/1.4037074>
- [10] Rackauckas, C. "A Comparison Between Differential Equation Solver Suites In MATLAB, R, Julia, Python, C, Mathematica, Maple, and Fortran", *The Winnower*, 5:e153459.98975, 2018
<https://doi.org/10.15200/winn.153459.98975>
- [11] Dormand, J. R., Prince, P. J. "A family of embedded Runge-Kutta formulae", *Journal of Computational and Applied Mathematics*, 6(1), pp. 19–26, 1980.
[https://doi.org/10.1016/0771-050X\(80\)90013-3](https://doi.org/10.1016/0771-050X(80)90013-3)
- [12] Kloda, L., Lenci, S., Warminski, J. "Hardening vs. softening dichotomy of a hinged-simply supported beam with one end axial linear spring: Experimental and numerical studies", *International Journal of Mechanical Sciences*, 178, 105588, 2020.
<https://doi.org/10.1016/j.ijmecsci.2020.105588>
- [13] Hartman, P. "A lemma in the theory of structural stability of differential equations", *Proceedings of the American Mathematical Society*, 11(4), pp. 610–620, 1960.
<https://doi.org/10.1090/S0002-9939-1960-0121542-7>
- [14] Perko, L. "Differential Equations and Dynamical Systems", *Texts in Applied Mathematics*, 7, Springer, 2001. ISBN: 978-1-4612-6526-9
<https://doi.org/10.1007/978-1-4613-0003-8>